A Comparative Study on the Dynamics of the Pacific-Japan (PJ) Teleconnection Pattern as Revealed in Reanalysis Datasets

Y. Kosaka[1], H. Nakamura[1, 2]
[1]Department of Earth and Planetary Science, The University of Tokyo, Japan
[2]Frontier Research Center for Global Change, JAMSTEC, Japan
Correspondence: ykosaka@eps.s.u-tokyo.ac.jp

INTRODUCTION

The Pacific-Japan (PJ) teleconnection pattern is one of the dominant atmospheric anomaly patterns that influence summertime weather conditions over the Far East. It is characterized by anomalous convective activity over the tropical Northwestern Pacific and a meridional dipole of anomalous circulation in the lower troposphere (Nitta 1987). Through their composite study based on the U.S. National Centers for Environmental Prediction (NCEP)-Department of Energy reanalysis dataset (NCEP-2; Kanamitsu et al. 2002) for the atmosphere, Kosaka and Nakamura (2006, hereafter KN06) have shown that the PJ pattern is characterized by zonally elongated, meridionally tilted vorticity anomalies that gain kinetic energy (*KE*) from the mean jet streams in the upper and lower troposphere and available potential energy (*APE*) as well from the vertically sheared time mean jets through dry energy conversions, in addition to moist *APE* generation with the anomalous convective activity. They concluded that the PJ pattern can be interpreted as a dynamical mode in the atmosphere inherent to the boundary region between the continental Asian summer monsoon to the west and the maritime North Pacific subtropical high to the east.

Evaluation of the *APE* generation requires a field of diabatic heating (Q), which can be obtained as a product of 6-hourly integrations of a weather forecast model used for a reanalysis system. Compared to wind or temperature fields, Q is less constrained by observations, and its quality should therefore be more dependent on specific schemes in a particular reanalysis system, including a parameterization of cumulus convection. It is therefore necessary to re-evaluate the energy generation and conversions associated with the PJ pattern, by applying the same analysis as in KN06 to other reanalysis datasets available, including the European Centre for Medium-Range Weather Forecasts (ECMWF) reanalysis (ERA-40; Uppala et al. 2005), the NCEP/National Center for Atmospheric Research reanalysis (NCEP-1; Kalnay et al. 1996) and the Japanese 25-year reanalysis (JRA-25; Onogi et al. 2007), which is known for improved representation of tropical precipitation and tropical cyclones. The aim of this study is to qualitatively confirm the results on the mechanism of the PJ pattern obtained by KN06 and to assess a degree of uncertainty in the evaluation of energetics for the PJ pattern among the four reanalysis datasets currently available.

DATASETS AND ANALYSIS METHODS

In addition to the four monthly-mean reanalysis datasets, i.e., NCEP-1, NCEP-2, ERA-40 and JRA-25, the Climate Prediction Center (CPC) Merged Analysis of Precipitation data (CMAP; Xie and Arkin 1997) are also used. For each of the datasets, a particular version of 2.5° × 2.5° horizontal resolution is chosen for a fair comparison, and anomaly fields have been defined for June, July and August (JJA) as departures from the 23-year (from 1979 to 2001) climatology for the respective calendar months.

The Q data consist of several components, including latent heat release due to convection and large-scale condensation, radiative heating and the effect of subgrid-scale turbulence, but their combination is not totally identical among datasets (e.g., shallow convective heating is not included in the JRA-25). For a fair comparison, the

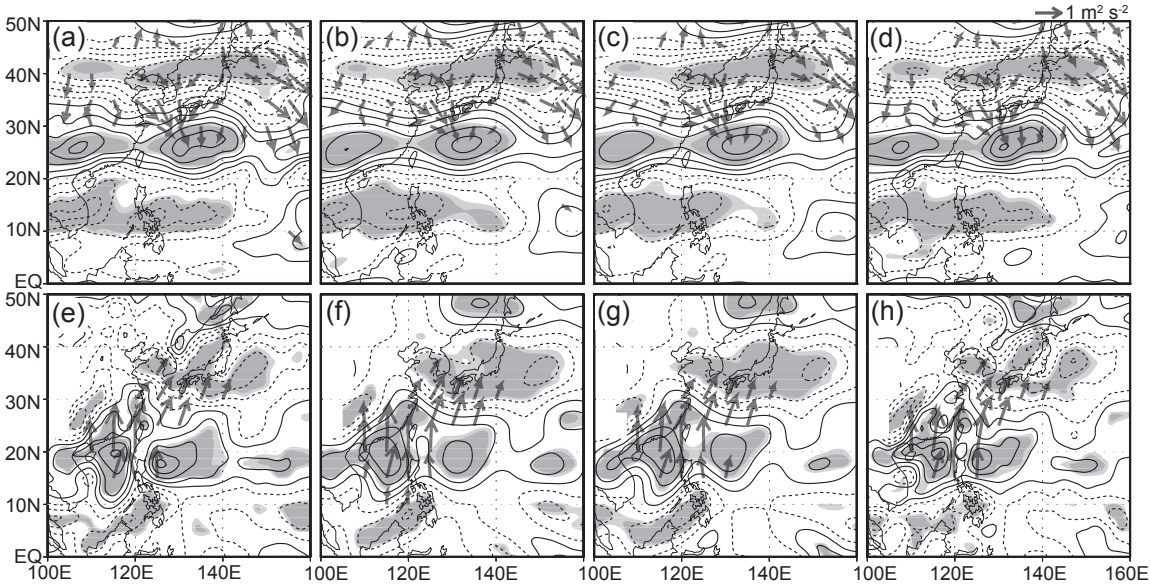

Figure 1 Composited vorticity anomalies ($\times 10^{-6}$ s^{-1}) at the (a-d) 150- and (e-h) 850-hPa levels based on the (left) JRA-25, (middle left) NCEP-2, (middle right) NCEP-1 and (right) ERA-40 for the 29 strongest monthly events of the PJ pattern with enhanced convective activity in a tropical domain [10°-20°N, 120°-130°E]. Contours are drawn with an interval of 1 (±0.5, ±1.5, ±2.5, …). Solid and dashed lines indicate the positive and negative values, respectively. Light and heavy shading represent the confidence levels of 90 and 95%, respectively, based on the *t*-statistic. Also shown with arrows is a Rossby wave-activity flux formulated by Takaya and Nakamura (2001).

total Q is used in this study, while only the component of deep convective heating is used in KN06. No Q fields are currently available for the authors in the ERA-40.

KN06 identified 32 monthly events of enhanced convection associated with the PJ pattern, based on the strongest negative outgoing longwave radiation (OLR) anomaly observed over [10°-20°N, 120°-130°E] for each of the 75 summer months (JJA) from 1979 to 2003, using the U.S. National Oceanic and Atmospheric Administration (NOAA) interpolated OLR data. In this study, 29 out of those 32 events (excluding three events in 2002 and 2003) were composited for each of the four datasets.

STRUCTURE OF THE PJ PATTERN

As revealed in Figs. 1 and 2, pronounced increase in precipitation over northern part of the South China Sea and to the east of the Philippines (Fig. 2) for the positive phase of the PJ pattern accompanies a meridional dipole of zonally-elongated vorticity anomalies (cyclonic anomalies around the region of enhanced convection and anticyclonic anomalies to their northeast) and an associated poleward wave-activity flux in the lower troposphere (Figs. 1e-h). In Figs. 1 (a-d), upper-tropospheric vorticity anomalies are organized into a tripole-like structure, with a quarter-wavelength meridional shift relative to their lower-tropospheric counterpart, generally accompanying an equatorward wave-activity flux. These features are the characteristics of the PJ pattern identified by KN06. The overall structure of the vorticity anomalies are similar in the composites based on the four reanalysis datasets. Finer structures are resolved in the JRA-25 and ERA-40, reflecting higher resolutions of the forecast models used in these reanalyses.

Figures 3 (a-d) compare the composited anomalies of precipitation. In each of the four datasets, enhanced precipitation is analyzed over northern part of the South China Sea and to the east of the Philippines, but its magnitude and detailed structure differ noticeably. The magnitude of the maximum anomaly in the JRA-25 (Fig. 3a) and ERA-40 (Fig. 3d) is almost the same as observed in CMAP (Fig. 2), although the anomalies in the JRA-25 are more localized and differ significantly over the South China Sea. The composited rainfall anomalies for the

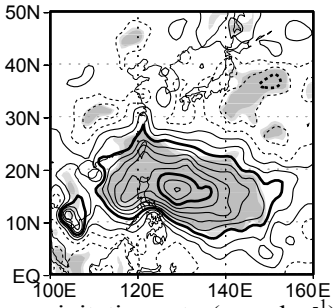

Figure 2 As in Fig. 1, but for CMAP precipitation rate (mm day^{-1}). Contours are drawn with an interval of 0.4 (±0.2, ±0.6, ±1, …).

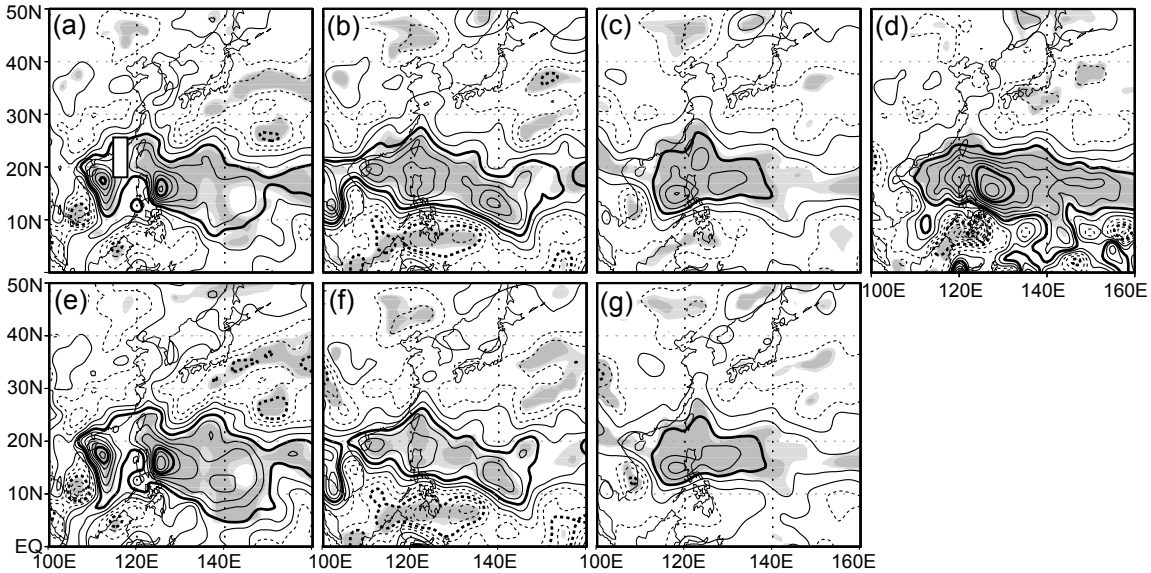

Figure 3 As in Fig. 1, but for (a-d) anomalous precipitation rate (mm day^{-1}) and (e-g) anomalous diabatic heating rate (K day^{-1}) at the 400-hPa level for the (left) JRA-25, (midde left) NCEP-2, (middle right) NCEP-1 and (right) ERA-40. Contours are drawn with intervals of (a-d) 0.4 (±0.2, ±0.6, ±1, …) and (e-g) 0.2(±0.1, ±0.3, ±0.5, …), with bold lines indicating (a-d) ±1, ±3, … and (e-g) ±0.5, ±1.5, ….

NCEP-2 (Fig. 3b) and NCEP-1 (Fig. 3c) are weaker than the CMAP anomalies (Fig. 2). Zonally-elongated negative precipitation anomalies to the south of the Philippines, which are, however, almost absent in the CMAP data, are much stronger in the NCEP-2 and ERA-40 than in the two other datasets.

The above features in the composited rainfall anomalies are reflected in the *Q* anomaly distribution (Figs. 3e-g) for the JRA-25, NCEP-2 and NCEP-1 datasets. The maximum reaches as much as ~2 K day^{-1} in the JRA-25 (Fig. 3e), while it is only ~1 K day^{-1} in the NCEP-2 (Fig. 3f) and NCEP-1 (Fig. 3g). Corresponding to the unrealistically reduced precipitation analyzed, negative diabatic heating anomalies to the south of the Philippines are much stronger in the NCEP-2 than in the NCEP-1 and JRA-25.

ENERGETICS

Following KN06, we evaluated the barotropic (*CK*) and baroclinic (*CP*) energy conversions and diabatic *APE* generation (*CQ*) as well, as follows:

$$CK = (v'^2 - u'^2)/2 \cdot (\partial\overline{u}/\partial x - \partial\overline{v}/\partial y) - u'v'(\partial\overline{u}/\partial y + \partial\overline{v}/\partial x)\,, \tag{1}$$

$$CP = -(f/\sigma)(v'T'\,\partial\overline{u}/\partial p - u'T'\,\partial\overline{v}/\partial p)\,, \tag{2}$$

and

$$CQ = (R/C_p)\,T'Q'/p\sigma\,, \tag{3}$$

Table 1. Time scales τ_{CK}, τ_{CP}, τ_{CQ}, τ_{dry} and τ_{moist} (days) with which horizontally integrated energy associated with the PJ pattern could be replenished through energy conversions and diabatic generation as in Eqs. (1)-(3), for the composited anomalies based on the four reanalysis datasets as indicated.

	JRA-25	NCEP-1	NCEP-2	ERA-40
τ_{CK}	58.2	40.4	47.8	52.0
τ_{CP}	16.8	15.6	16.5	18.1
τ_{CQ}	15.5	-31.5	-29.9	
τ_{dry}	30.0	24.3	26.9	29.3
τ_{moist}	40.7	-76.0	-73.0	

respectively, based on the composited anomalies for the 29 events of the PJ pattern. In Eqs. (1)-(3), σ denotes the stability parameter $\sigma = R\overline{T}/C_p p - \partial\overline{T}/\partial p$, and overbars and primes represent the climatological-mean fields and the PJ-associated anomalies, respectively. Other notation is standard. Efficiencies of the conversions and generation are evaluated as the time scales given by

$$\tau_{CK} = \langle KE \rangle_{\mathrm{NH}} / \langle CK \rangle_{\mathrm{WP}} , \tag{4}$$

$$\tau_{CP} = \langle APE \rangle_{\mathrm{NH}} / \langle CP \rangle_{\mathrm{WP}} , \tag{5}$$

$$\tau_{CQ} = \langle APE \rangle_{\mathrm{NH}} / \langle CQ \rangle_{\mathrm{WP}} , \tag{6}$$

$$\tau_{\mathrm{dry}} = \langle KE + APE \rangle_{\mathrm{NH}} / \langle CK + CP \rangle_{\mathrm{WP}} , \tag{7}$$

and

$$\tau_{\mathrm{moist}} = \langle KE + APE \rangle_{\mathrm{NH}} / \langle CQ \rangle_{\mathrm{WP}} , \tag{8}$$

based on the composites for the individual reanalysis datasets. Here, $\langle\ \rangle_{\mathrm{NH}}$ and $\langle\ \rangle_{\mathrm{WP}}$ denote spatial integrations almost over the entire Northern Hemisphere (5°-85°N) and over the western North Pacific (5°-60°N, 100°-150°E), respectively, both after integrated vertically from the surface to the 100-hPa level. Consistently with the structural similarity of the PJ-associated circulation anomalies, the efficiencies in the dry energy conversions are overall comparable among the four datasets, though slightly less efficient in the JRA-25 and ERA-40 data (Table 1). *CP* is as three times as efficient as *CK*, and the two dry conversions combined can replenish the total energy associated with the PJ anomalies within a month. The most striking feature in Table 1 is differences in the moist diabatic *APE* generation among the datasets. While *CQ* based on the JRA-25 is efficient enough to replenish the total energy within a time scale comparable to that for the dry conversions, the net generation is negative when based on either of the NCEP-1 and NCEP-2.

The substantial differences in the *CQ* efficiency can be understood by comparing the composited temperature (*T*) anomalies, as involved in the energetics through Eqs. (2) and (3). As shown in Figs. 4 (a-d), a band of significant warm anomalies centered at 40°N is common to the four datasets, with almost the same magnitude. Since it is these midlatitude anomalies that account primarily for the positive $\langle CP \rangle_{\mathrm{WP}}$, the result is consistent with the comparable efficiency assessed as τ_{CP}. Meanwhile, the tropical anomalies are distributed in rather different manners. In the JRA-25 (Fig. 4a) and ERA-40 (Fig. 4d), significant warm anomalies are evident around the northern Philippines, where enhanced *Q* is observed in the JRA-25. In contrast, they are weaker and less significant in the NCEP-2 (Fig. 4b) and NCEP-1 (Fig. 4c). In these NCEP datasets, significant cool anomalies prevail to the south or southwest of the Philippines, where the unrealistic reduction in precipitation is analyzed, especially for the NCEP-2 (Fig. 2b). Although the *T* differences in the tropics are rather weak (max. ~0.3 K) and associated with no significant wind differences, they do lead to the substantial differences in the energetics as in Table 1. Additionally, in most of the 29 monthly events of enhanced convection composited, mid-tropospheric warm anomalies over [15°-25°N, 110°-130°E] are stronger in the JRA-25 and ERA-40 than in the NCEP-1 or NCEP-2, indicating that these differences are unlikely a statistical artifact.

In Figs. 4 (i-k), where the *CQ* distributions based on those three reanalysis datasets are compared, *CQ* associ-

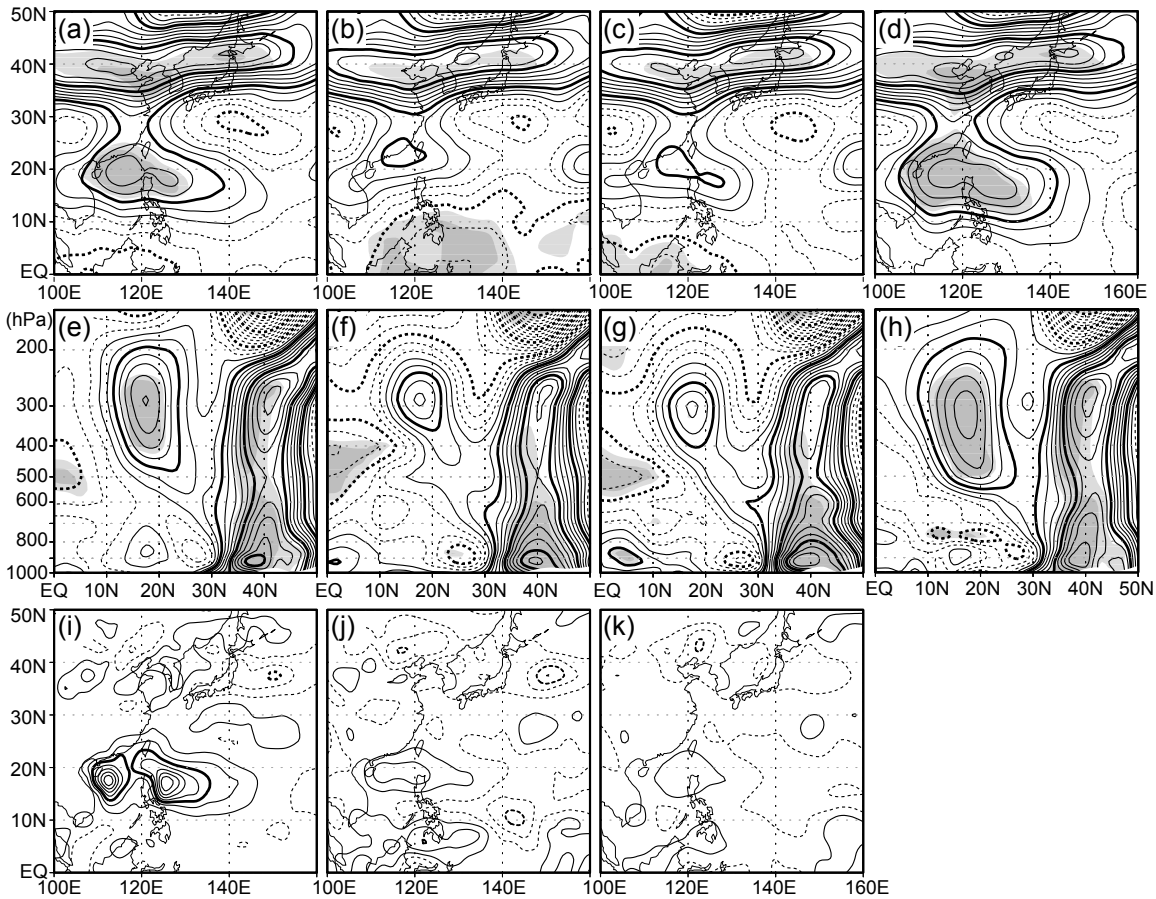

Figure 4 As in Fig. 3, but for (a-h) anomalous temperature (K) (a-d) at the 400-hPa level and (e-h) along 125°E and (i-k) local diabatic *APE* generation (W m^{-2}) integrated from the surface to the 100-hPa level. Contours are drawn with intervals of (a-h) 0.04 (±0.02, ±0.06, ±0.1, …) and (i-k) 0.02 (±0.01, ±0.03, ±0.05, …), with bold lines indicating (a-h) ±0.1, ±0.3, ±0.5, … and (i-k) ±0.05, ±0.15, ±0.25, ….

ated with enhanced convection around the northern Philippines is apparently stronger in the JRA-25 (Fig. 4i), owing to the stronger heating and warm anomalies. In the NCEP-2 (Fig. 4j) and NCEP-1 (Fig. 4k), another area of positive *CQ* is found to the south of the Philippines associated with the negative *Q* anomalies acting on the cool anomalies. The positive but relatively weak *CQ* is canceled out partially by negative *CQ* found to the east of the Philippines. This negative *CQ* arises from positive *Q* anomalies extending into the tropical region of cool anomalies, both of which are particularly strong in the NCEP-2. In other words, anomalous *Q* and *T* are stronger and spatially more coherent in the JRA-25. Though similarity of temperature anomaly distribution to that in the JRA-25 is higher for the NCEP-1, weaker and narrower distribution of anomalous *Q* in the NCEP-1 weakens *CQ*, yielding $\langle CQ \rangle_{\mathrm{WP}}$ as inefficient as in the NCEP-2 (Table 1).

Meridional sections of the composited anomalies (Figs. 4e-h) show that the upper-level warm anomalies around 20°N are statistically significant and deep in the JRA-25 (Fig. 4e) and ERA-40 (Fig.4h). In the NCEP-2 (Fig. 4f) and NCEP-1 (Fig. 4g), in contrast, they tend to be weaker, shallower and less significant, lowering their spatial correlation with *Q* anomalies and the resultant *CQ*. Additionally, the mid-tropospheric cold anomalies near the equator are stronger and more significant in the NCEP datasets. The shallower upper-level *T* anomalies around 20°N and the stronger mid-tropospheric anomalies around the equator in the NCEP datasets can also be found in one-point correlation maps of *T* with a reference point at (20°N, 125°E, 300 hPa; supplement 2), indicating that those features are robust.

CONCLUDING REMARKS

In the present study, we have shown that the PJ-associated anomalous circulation manifested as vorticity anomalies is overall similar among the four reanalysis datasets, i.e., JRA-25, NCEP-1, NCEP-2 and ERA-40, and so are the *KE* and *APE* conversions from the climatological-mean state. We have demonstrated, however, that the associated temperature and convection anomalies exhibit considerable discrepancies. In the JRA-25 and ERA-40, the composited anomalies of temperature and precipitation tend to be more coherent than in the NCEP-1 and NCEP-2, suggesting that some systematic errors might be included in the latter. Microwave-measured precipitable water data assimilated in the JRA-25 and ERA-40 and realistic surface-pressure bogus fields for tropical cyclones in the former are likely to contribute to the improved representation of moist processes.

Our evaluation confirms the results of KN06 based on the NCEP-2 that the PJ pattern has characteristics of a dry dynamical mode in the particular configuration of the summertime mean flow between the Asian monsoon and the North Pacific subtropical high. However, our analysis based on the JRA-25 also indicates that the contribution from the moist convective *APE* generation, which is not particularly emphasized in KN06, can be comparable to that from the dry energy conversions in maintaining the PJ pattern. In recognition of certain uncertainties in moist processes in the reanalysis datasets, discussion on the moist energetics of the PJ pattern based on reanalysis data should remain qualitative. More quantitative discussion on the energetics of the PJ pattern requires further improvement in quality of reanalysis data.

ACKNOWLEDGMENTS

This study is supported by the Grant-in-Aid #18204044 by the Japanese Ministry of Education, Culture, Sports, Science and Technology, and also by the Global Environment Research Fund (S-5) of the Ministry of the Environment, Japan. The JRA-25 dataset is available through the cooperative research project of the JRA-25 long-term reanalysis by the Japan Meteorological Agency and the Central Research Institute of Electric Power Industry. The CMAP, NCEP-1 and NCEP-2 datasets have been obtained from the web site of the NOAACIRES Climate Diagnostics Center, http://www.cdc.noaa.gov/. The ERA-40 dataset has been provided by the ECMWF Data Server from their web site at http://data.ecmwf.int/data/.

REFERENCES

Kalnay, E., M. Kanamitsu, R. Kistler, W. Collins, D. Deaven, L. Gandin, M. Iredell, S. Saha, G. White, J. Woollen, Y. Zhu, M. Chelliah, W. Ebisuzaki, W. Higgins, J. Janowiak, K. C. Mo, C. Ropelewski, J. Wang, A. Leetmaa, R. Reynolds, R. Jenne, and D. Joseph, 1996: The NCEP/NCAR 40-year reanalysis project. Bull. Amer. Meteor. Soc., **77**, 437-471.

Kanamitsu, M., W. Ebisuzaki, J. Woollen, S.-K. Yang, J. J. Hnilo, M. Fiorino, and G. L. Potter, 2002: NCEP-DOE AMIP-II reanalysis (R-2). Bull. Amer. Meteor. Soc., **83**, 1631-1643.

Kosaka, Y., and H. Nakamura, 2006: Structure and dynamics of the summertime Pacific-Japan teleconnection pattern. Quart. J. Roy. Meteor. Soc., **132**, 2009-2030.

Nitta, T., 1987: Convective activities in the tropical Western Pacific and their impact on the Northern Hemisphere summer circulation. J. Meteor. Soc. Japan, **65**, 373-390.

Onogi, K., J. Tsutsui, H. Koide, M. Sakamoto, S. Kobayashi, H. Hatsushika, T. Matsumoto, N. Yamazaki, H. Kamahori, K. Takahashi, S. Kadokura, K. Wada, K. Kato, R. Oyama, T. Ose, N. Mannoji, and R. Taira, 2007: The JRA-25 reanalysis. J. Meteor. Soc. Japan, **85**, 369-432.

Takaya, K., and H. Nakamura, 2001: A formulation of a phase-independent wave-activity flux for stationary and migratory quasigeostrophic eddies on a zonally varying basic flow. J. Atmos. Sci., **58**, 608-627.

Uppala, S. M., P. W. K_allberg, A. J. Simmons, U. Andrae, V. da Costa Bechtold, M. Fiorino, J. K. Gibson, J. Haseler, A. Hernandez, G. A. Kelly, X. Li, K. Onogi, S. Saarinen, N. Sokka, R. P. Allan, E. Andersson, K. Arpe, M. A. Balmaseda, A. C. M. Beljaars, L. van de Berg, J. Bidlot, N. Bormann, S. Caires, F. Chevallier, A. Dethof, M. Dragosavac, M. Fisher, M. Fuentes, S. Hagemann, E. Holm, B. J. Hoskins, L. Isaksen, P. A. E. M. Janssen, R. Jenne, A. P. McNally, J.-F. Mahfouf, J.-J. Morcrette, N. A. Rayner, R. W. Saunders, P. Simon, A. Sterl, K. E. Trenberth, A. Untch, D. Vasiljevic, P. Viterbo, and J. Woollen, 2005: The ERA-40 re-analysis. Quart. J. Roy. Meteor. Soc., **131**, 2961-3012.

Xie, P., and P. A. Arkin, 1997: Global Precipitation: A 17-year monthly analysis based on gauge observations, satellite estimates and numerical model outputs. Bull. Amer. Meteor. Soc., **78**, 2539-2558.